Chen et al. Nanoscale Research Letters (2018) 13:140
https://doi.org/10.1186/s11671-018-2556-8

Nanoscale Research Letters

NANO EXPRESS Open Access

Effect of Different $CH_3NH_3PbI_3$ Morphologies on Photovoltaic Properties of Perovskite Solar Cells

Lung-Chien Chen[1*], Kuan-Lin Lee[1], Wen-Ti Wu[2], Chien-Feng Hsu[1], Zong-Liang Tseng[1], Xiao Hong Sun[3] and Yu-Ting Kao[1]

Abstract

In this study, the perovskite layers were prepared by two-step wet process with different CH_3NH_3I (MAI) concentrations. The cell structure was glass/FTO/TiO_2-mesoporous/$CH_3NH_3PbI_3$ ($MAPbI_3$)/spiro-OMeTAD/Ag. The $MAPbI_3$ perovskite films were prepared using high and low MAI concentrations in a two-step process. The perovskite films were optimized at different spin coating speed and different annealing temperatures to enhance the power conversion efficiency (PCE) of perovskite solar cells. The PCE of the resulting device based on the different perovskite morphologies was discussed. The PCE of the best cell was up to 17.42%, open circuit voltage of 0.97 V, short current density of 24.06 mA/cm^2, and fill factor of 0.747.

Keywords: Solar cells, Perovskite, $CH_3NH_3PbI_3$, Two-step deposition

Background

Organic perovskite films have drawn much attention for better power conversion efficiency in thin film-type solar cells [1–3]. Many growth methods have been developed to prepare perovskite films. Among them, a two-step method is widely used due to its high film quality and reliability of the resulting films [4, 5]. The perovskite is a versatile material prepared from abundant and low-cost compounds, also having unique optical and long excitonic properties, as well as good electrical conductivity. The power conversion efficiency (PCE) of perovskite solar cells has been improved from 3.8 to 22.1% in recent years.

There are two methods for preparing perovskite films: one-step and two-step methods for $CH_3NH_3PbI_3$ films; the one-step method is that the PbI_2 and CH_3NH_3I (MAI) are mixed in a solvent to form $CH_3NH_3PbI_3$ films, such as vacuum flash-assisted solution processes, [5] solvent engineering, [6] humidity control, [7, 8] and mixed precursors [9]. Although the one-step method is the most widely used method to prepare the perovskite solar cells, it needs to dissolve both the organic and the inorganic precursors, which reduced the control of the film property including thickness, uniformity, and morphology. The two-step method is that the PbI_2 films were first prepared and subsequently reacted with MAI to form $CH_3NH_3PbI_3$ films. In 2013, Bi et al. [10] first showed the PCE of 9.5% by using two-step method. They prepare PbI_2 films on mesoporous TiO_2 films the by spin coating a PbI_2 solution in dimethylformamide (DMF). After drying, the films were dipped in a solution of MAI in 2-propanol to form high-quality $CH_3NH_3PbI_3$ films for the perovskite solar cells. In the same year, Burschka et al. [11] showed the certification for the perovskite solar cells prepared by the two-step method and confirmed a power conversion efficiency of 14.14% measured under standard AM1.5G reporting conditions. After that, many studies using the two-step method to improve the PCE of the perovskite solar cells were reported [12–18]. Moreover, long-term stability is important for the future application of perovskite devices. Several nanostructures, like carbon layer [19] and graphene oxide-modified PEDOT:PSS [20], have been used to suppress degradation in the device and

* Correspondence: ocean@ntut.edu.tw
[1]Department of Electro-Optical Engineering, National Taipei University of Technology, 1, Section 3, Chung-Hsiao E. Road, Taipei 106, Taiwan
Full list of author information is available at the end of the article

improve their performance. However, few studies discuss the effect of different surface morphology on photovoltaic properties of perovskite solar cells.

In this study, we controlled the grain size and morphology of $CH_3NH_3PbI_3$ by different MAI concentration, annealing, and two-step. Moreover, it was found that the surface morphology of $CH_3NH_3PbI_3$ films using low MAI concentrations showed large perovskite grains, but the morphology of $CH_3NH_3PbI_3$ films using high MAI concentrations showed dense and smooth grains. Photovoltaic conversion efficiency of the resulting cells based on the different perovskite morphologies was analyzed using XRD spectra, SEM, UV-vis absorption spectroscopy, and photoluminescence (PL) spectra. As a result, the power conversion efficiency of the best cell was up to 17.42%.

Methods

In this study, fluorine-doped tin oxide (FTO) glass as substrate was cut into small pieces with a size of 1.5 × 1.5 cm^2. The FTO glass substrates were thoroughly cleaned with acetone, ethanol, and deionized (DI) water in an ultrasonic oscillator for 5 min, respectively, and dried with nitrogen. A 50-nm compact TiO_2 blocking layer was first deposited onto the surface of the precleaned FTO substrate by spray pyrolysis method at a temperature of 500 °C, using a solution of 0.2 M Ti-isopropoxide and 2 M acetylacetone in isopropanol. The mesoporous layer TiO_2 was deposited by spin coating a diluted paste (Dyesol 18NR-T), followed by heating to 450 °C. Next, the two-step method was employed to deposit a perovskite layer. PbI_2 (Alfa Aesar, 99.9985% purity) was deposited via spin coating from a solution 1 mol/L PbI_2 in dimethylformamide (DMF) that was heated to 70 °C, with a spin coating speed of 7000 rpm. $MAPbI_3$ was formed by dipping the slide into a 10-mg/mL MAII in isopropanol (IPA) solution with different concentrations for 30 s. After removing the excess IPA, the perovskite films were then placed on a hot plate set at 100 °C for 20 min. The composition of hole transport material was 0.170 M 2,2′,7,7′-tetrakis(*N*,*N*-di-p-methoxyphenyl-amine)-9,99-spirobifluorene (spiro-OMeTAD, Lumtec), with the addition of 60 mM bis(trifluoromethane)sulfonimide lithium salt (LiTFSI, 99.95%, Aldrich) and 200 mM 4-tert-butylpyridine (TBP, 99%, Aldrich). The $CH_3NH_3PbI_3$/TiO_2 films were coated with a spiro-OMeTAD solution using the spin coating method at 4000 rpm. For the electrical contact, a 100-nm Ag film was deposited onto the solar cell by thermal evaporation. The resultant device was composed of silver/spiro-OMeTAD/$MAPbI_3$/TiO_2 mesoporous layer/TiO_2 compact layer/FTO/glass. Figure 1 schematically depicts the complete structure. The current density-voltage (J-V) curves of solar cells were obtained using a source measurement unit (Keithly 2400). The photoluminescence spectra of the $CN_3NH_3PbI_3$/glass samples were measured using a microscope-based spectrometer. The active area of the devices is 2 × 5 mm^2 by a shadow mask. The X-ray diffraction patterns of the $CN_3NH_3PbI_3$/glass samples were recorded using a theta-2theta mode.

Results and Discussion

Figure 2 shows the top-view (left column) and cross-sectional (right column) SEM images of the $MAPbI_3$ perovskite films prepared by low-concentration MAI

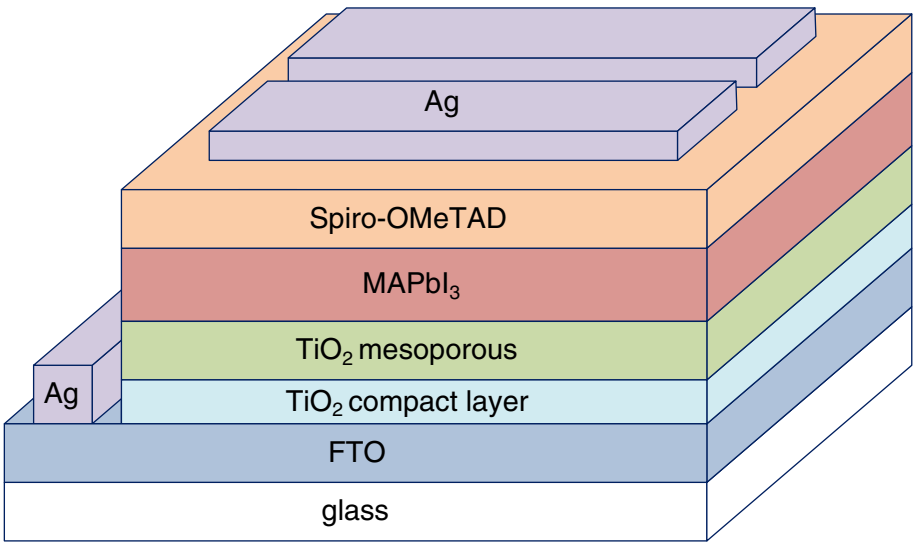

Fig. 1 Schematic of the complete structure

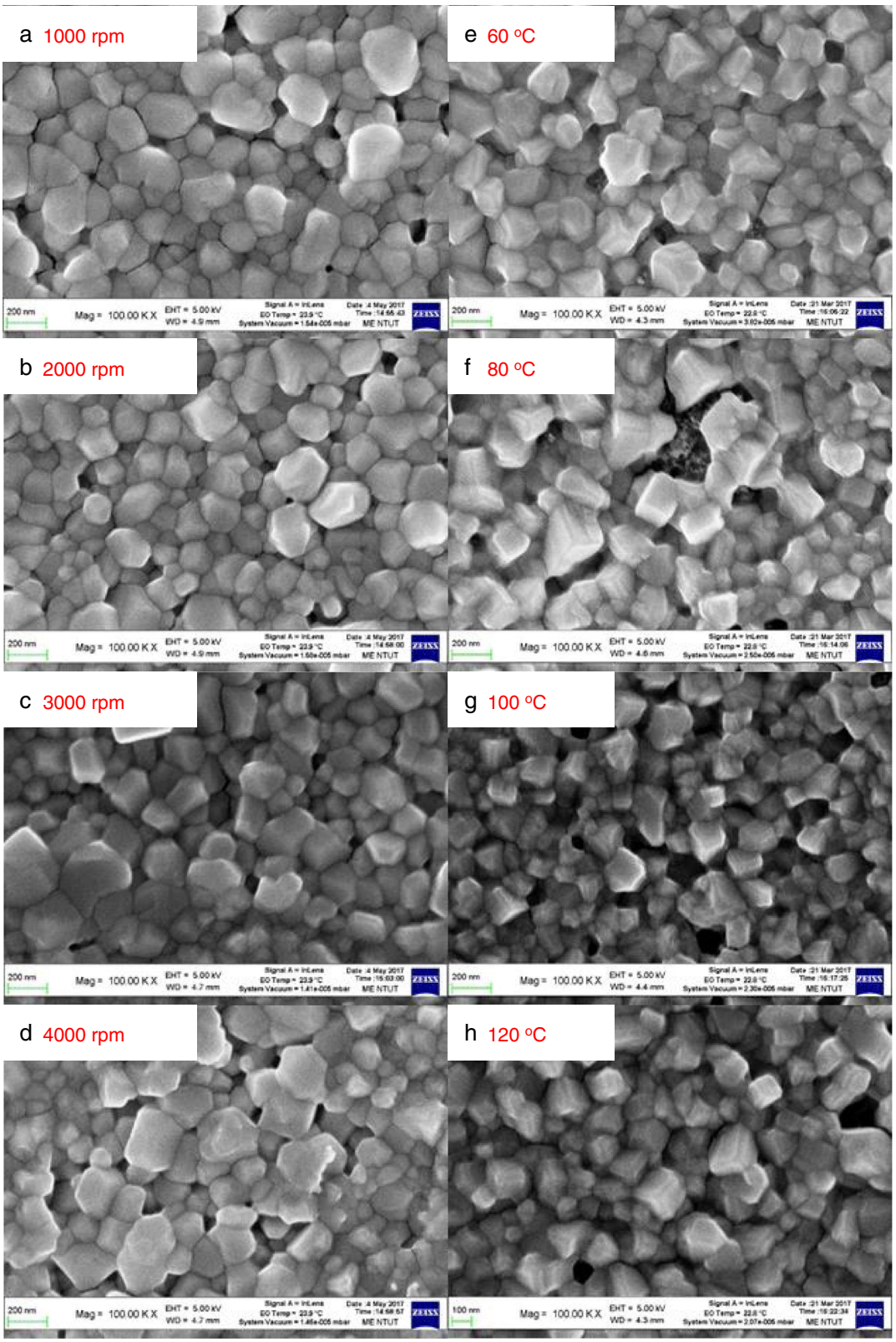

Fig. 2 Top-view SEM images of the $MAPbI_3$ perovskite films prepared by low-concentration MAI (10 mg/mL) with **a-d** various spin coating speeds and **e-h** annealing treatments

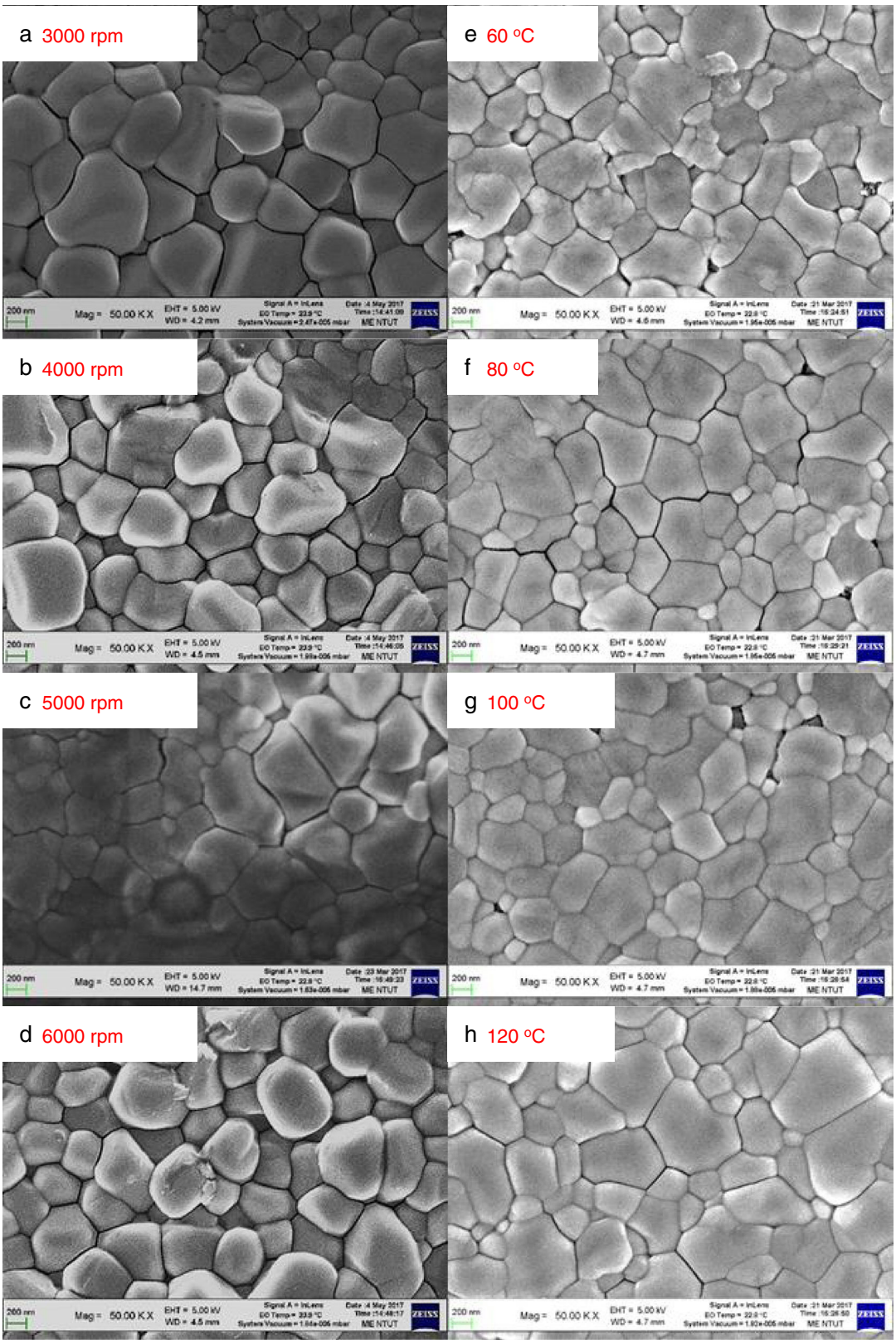

Fig. 3 Top-view SEM images of the $MAPbI_3$ perovskite films prepared by high-concentration MAI (10 mg/mL) with **a-d** various spin coating speeds and **e-h** annealing treatments

(10 mg/mL) and underwent annealing treatment at different temperatures. It was found that there is a large amount of perovskite particles on the surface and have a tetragonal morphology, as shown in Fig. 2a. The particles size and surface morphology of the perovskite films prepared by low-concentration MAI are similar for all samples.

Figure 3 shows the top-view (left column) and cross-sectional (right column) SEM images of the $MAPbI_3$ perovskite films prepared by high-concentration MAI (40 mg/mL) and underwent annealing treatment at different temperatures. Perovskite prepared by high-concentration MAI shows tetragonal crystals, the average $MAPbI_3$ domain size from about 200 nm to about 600 nm, as shown in Fig. 3. The morphology is different to that of the perovskite prepared by low-concentration MAI. It was found that there are some PbI_2 grains on the surface of the $MAPbI_3$ perovskite film with 60 °C annealing. Those are residues caused by the incomplete reaction. The domain size and surface morphology of the perovskite films prepared by high-concentration MAI are similar for all samples.

Figure 4 shows the XRD patterns of the $MAPbI_3$ films prepared by (a) low- and (b) high-concentration MAI with different annealing temperatures. As shown in Fig. 4a, two main diffraction peaks are observed at 12.6° and 14.4°, corresponding to PbI_2 (001) and $MAPbI_3$ (110) phases, respectively. The intensity of the PbI_2 (001) peak is higher than that of the $MAPbI_3$ (110) peak when the annealing temperature of the $MAPbI_3$ film increases up to 120 °C. The $MAPbI_3$ film is decomposed into a bi-phase film of the MAI and PbI_2, leading to poor efficiency of the perovskite solar cells. Similarly, as shown in Fig. 4b, as the annealing temperature is 60 °C, two main diffraction peaks are observed at 12.8° and 14.3°, corresponding to PbI_2 (001) and $MAPbI_3$ (110) phases, respectively. However, the single peak corresponding to the $MAPbI_3$ (110) phase is observed when the annealing temperature of the $MAPbI_3$ film increases up to over 80 °C. The MAI and PbI_2 are formed into the $MAPbI_3$ film, completely.

The intensity of photoluminescence (PL) spectrum is related to the lifetime of an exciton in the perovskite film and in the interface between TiO_2 and perovskite films. The lifetime of the exciton is longer, and the intensity of PL spectrum is stronger; the decomposition rate of an exciton in the interface between TiO_2 and perovskite films is faster, and the intensity of PL spectrum is weaker. Figure 5 plots PL spectra of the $MAPbI_3$ prepared by low- and high-concentration MAI with various spin coating speeds and annealing temperatures. As shown in Fig. 5a, b, the optimum spin coating speed and annealing temperature for the $MAPbI_3$ prepared by low-concentration MAI are 2000 rpm and 100 °C, respectively. On the other hand, as shown in Fig. 5c, d, the optimum spin coating speed and annealing temperature for the $MAPbI_3$ prepared by high-concentration MAI are 4000 rpm and 120 °C, respectively.

Figure 6 shows the SEM images of the $MAPbI_3$ perovskite films with low- and high-concentration MAI solution under optimum conditions, respectively. The surface morphology of the $MAPbI_3$ perovskite films with low-concentration MAI is rougher than that of the $MAPbI_3$ perovskite films with high-concentration MAI. The grain of the latter is compact and smooth. Also, the coverage rate of the surface of the latter is better than that of the former.

Figure 7a shows the PL spectra of the $MAPbI_3$ films with different MAI concentrations. The peak position of PL spectrum increases from 768 to 773 nm when the MAI concentration increases from 10 to 40 mg/mL. The redshift might be associated with the reaction of PbI_2 and MAI [21]. As the PbI_2 film is reacted with the MAI solution and formed

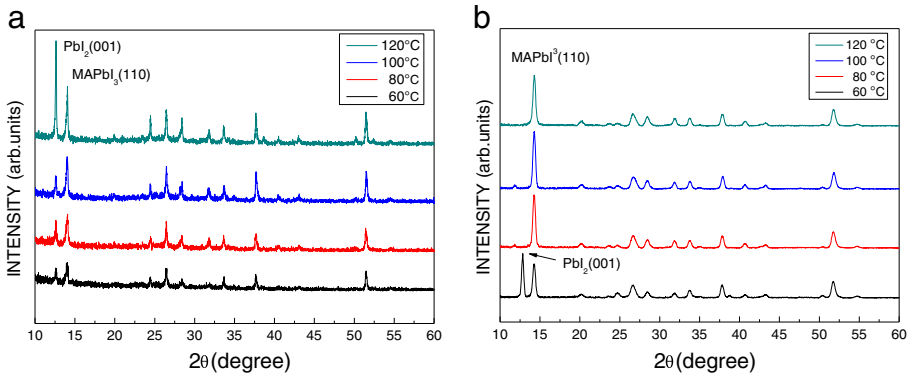

Fig. 4 XRD patterns of the $MAPbI_3$ films with **a** low- and **b** high-concentration MAI

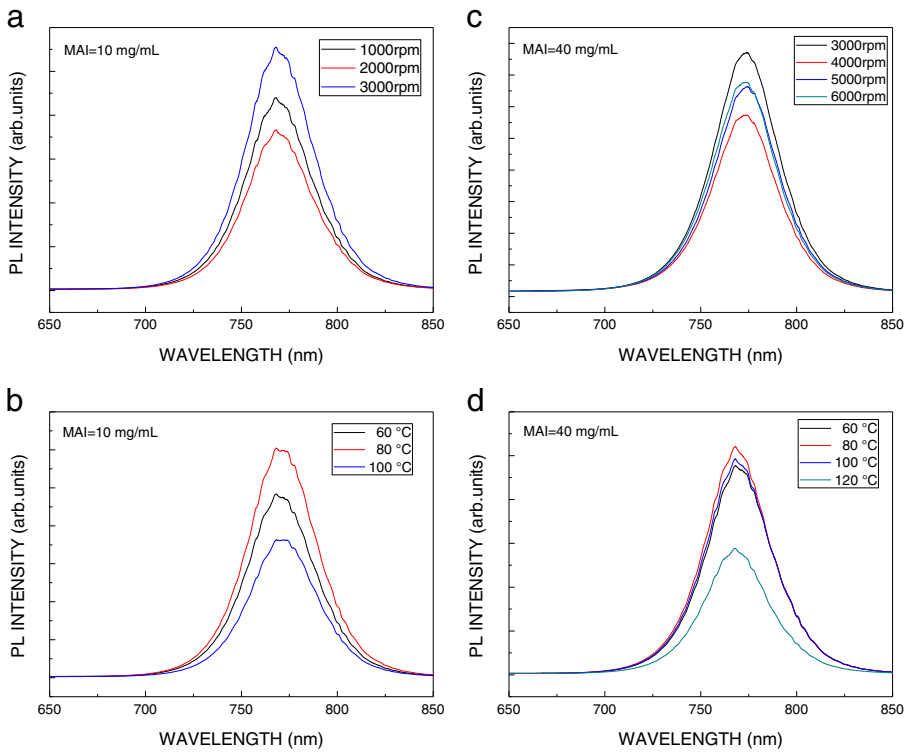

Fig. 5 PL spectra of $MAPbI_3$ prepared by low-concentration MAI with **a** various spin coating speeds and **b** annealing temperatures and prepared by high-concentration MAI with **c** various spin coating speeds and **d** annealing temperatures

the $MAPbI_3$ perovskite film, the band gap is shifted toward 1.55 eV. Also, the intensity of PL spectrum of the $MAPbI_3$ perovskite film using high MAI concentration is decay. To explore the original cause, time-resolved photoluminescence (TRPL) was employed to study the lifetime of the excitons. Therefore, the excitons can be quickly extracted to the FTO substrate, for the $MAPbI_3$ perovskite film using high MAI concentration. According to the TRPL spectra shown in Fig. 7b, the lifetime of the MAI perovskite films prepared by low and high concentration is 25 and 14 ns, respectively. It can clearly be seen that the exciton lifetime of the MAI perovskite films prepared by high MAI concentration is relatively short, which can be used to explain why the decomposition rate of the excitons is faster. The

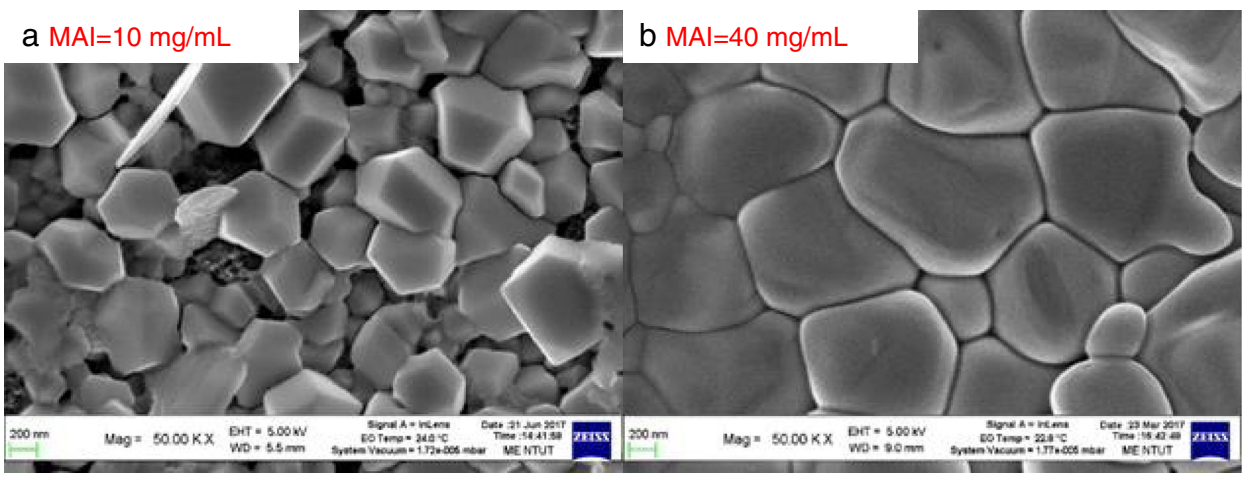

Fig. 6 SEM images of the $MAPbI_3$ perovskite films with **a** low- and **b** high-concentration MAI solution under optimum conditions, respectively

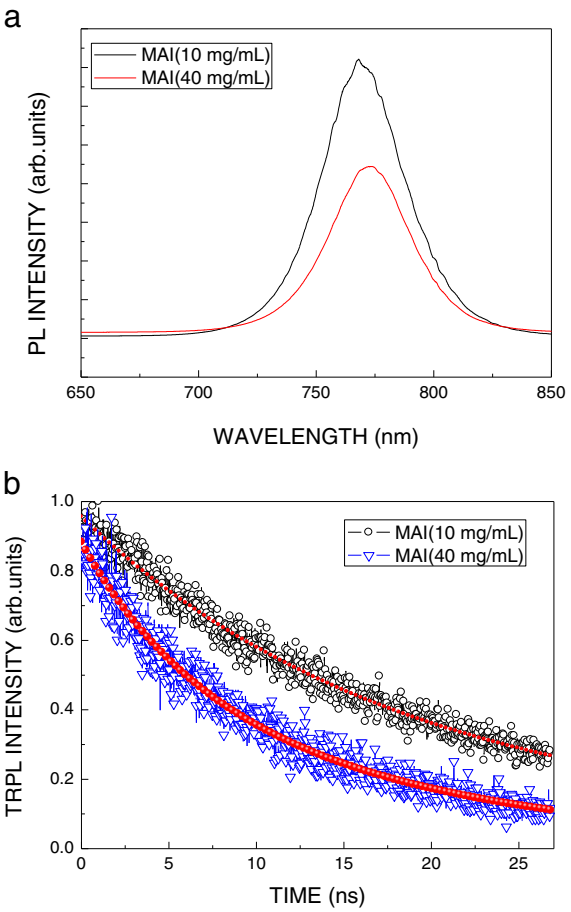

Fig. 7 **a** PL and **b** TRPL spectra of $MAPbI_3$ films with different concentrations

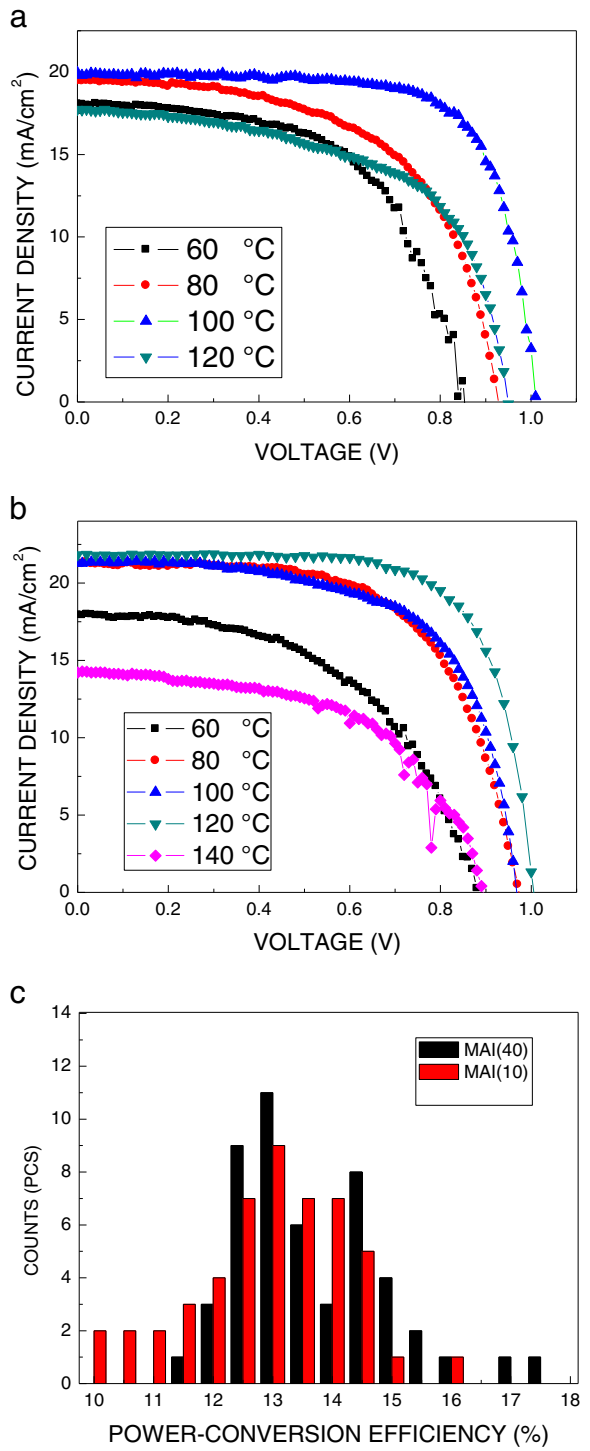

Fig. 8 J-V curves of the perovskite solar cells prepared using **a** low-concentration MAI and **b** high-concentration MAI with different annealing temperatures. **c** Histograms of PCE of the perovskite solar cells prepared by high-concentration MAI under the optimum process condition for 50 devices

interface between of TiO_2 and perovskite prepared by high MAI concentration is smooth, such that the excitons are separated and extracted quickly to the FTO substrate, as shown in Fig. 7b. In addition, it is possible to improve the film quality, resulting in an increase in the speed of the electrons decomposition.

Figure 8a, b plots the J-V curves of the perovskite solar cells prepared by low- and high-concentration MAI with different annealing temperatures, respectively. To compare the short-circuit current density Jsc, the perovskite solar cells prepared by high-concentration MAI are higher around 2 mA/cm^2 than that of the cells prepared by low-concentration MAI. This may be contributed by better quality of the perovskite films prepared by high-concentration MAI, such that it has a higher absorbance, resulting in a higher photocurrent. Besides, the charge transfer resistance in the perovskite films prepared by high-concentration MAI is small due to the smooth morphology. The films with the smooth morphology can not only increase the contact area between

perovskite film and spiro-MeTAD film but also enhance the photoelectric conversion efficiency of solar cells [22, 23]. On the other hand, the cells prepared by low-concentration MAI show high Voc. It may be caused by PbI_2 residues in the perovskite thin film [22, 23]. To check the reproducibility of performance, power conversion efficiency (PCE) is compared using histograms obtained from 50 perovskite devices prepared by low- and high-concentration MAI, as shown in Fig. 8c. As can be seen from the results, the devices performed extremely well. The average PCE of the perovskite solar cells prepared by low- and high-concentration MAI is 13 and 13.7% with a standard deviation of 1.293 and 1.275%, respectively. As shown in Fig. 8c, more than 75% of the cells show PCE above 13% under one sun conditions, for the perovskite solar cells prepared by high-concentration MAI. That indicates good reproducibility. The optimum results show the power conversion efficiency of 17.42%, open-circuit voltage of 0.97 V, current density of 24.06 mA/cm^2, and fill factor of 0.747.

Conclusions

In this study, the perovskite films prepared by high-concentration MAI were used to form solar cells. The effects of different morphologies of the films on the solar cells were investigated. The J-V characteristic curve of perovskite solar cells was used to improve the photoelectric conversion efficiency. The results show that the power conversion efficiency was up to 17.42%, open circuit voltage of 0.97 V, current density of 24.06 mA/cm^2, and fill factor of 74.66% was the best characteristic.

Abbreviations

FTO: Fluorine-doped tin oxide; J-V: Current density-voltage; MAI: CH_3NH_3I; $MAPbI_3$: $CH_3NH_3PbI_3$; PCE: Power conversion efficiency; PL: Photoluminescence; SEM: Scanning electron microscope; TRPL: Time-resolved photoluminescence; XRD: X-ray diffractometer

Funding

The authors gratefully acknowledge the financial support from the Ministry of Science and Technology of the Republic of China under Contract No. MOST 106-2221-E-027-091.

Authors' Contributions

LCC wrote the paper, designed the experiments, and analyzed the data. KLL, CFH, ZLT, and YTK prepared the samples and did all the measurements. WTW and XHS made the discussion and suggested parameter. All authors read and approved the final manuscript.

Ethics Approval and Consent to Participate

Not applicable.

Competing Interests

The authors declare that they have no competing interests.

Publisher's Note

Author details

[1]Department of Electro-Optical Engineering, National Taipei University of Technology, 1, Section 3, Chung-Hsiao E. Road, Taipei 106, Taiwan. [2]Institute of Chemistry, Academia Sinica, 128, Sec. 2, Academia Rd., Nankang, Taipei 115, Taiwan. [3]Henan Key Lab of Laser and Opto-electric Information Technology, School of Information Engineering, Zhengzhou University, Science Road 100, Zhengzhou, Henan, China.

Received: 20 January 2018 Accepted: 27 April 2018
Published online: 08 May 2018

References

1. Dubey A, Adhikari N, Mabrouk S, Wu F, Chen K, Yang S, Qiao Q (2018) A strategic review on processing routes towards highly efficient perovskite solar cells. J Mater Chem A 6(6):2406–2431
2. Dubey A, Adhikari N, Venkatesan S, Gu S, Khatiwada D, Wang Q, Mohammad L, Kumar M, Qiao Q (2016) Solution processed pristine PDPP3T polymer as hole transport layer for efficient perovskite solar cells with slower degradation. Sol Energy Mater Sol Cells 145:193–199
3. Tseng Z-L, Chiang C-H, Wu CG (2015) Surface engineering of ZnO thin film for high efficiency planar perovskite solar cells. Sci Rep 5:13211
4. Jeon N-J, Noh J-H, Kim Y-C, Yang W-S, Ryu S, Seok SI (2014) Solvent engineering for high-performance inorganic–organic hybrid perovskite solar cells. Nat Mater 13:897–903
5. Li X, Bi D, Yi C, Décoppet J-D, Luo J, Zakeeruddin S-M, Hagfeldt A, Grätzel M (2016) A vacuum flash–assisted solution process for high-efficiency large-area perovskite solar cells. Science 09:58–62
6. Wu W-Q, Chen DH, McMaster WA, Cheng Y-B, Caruso RA (2017) Solvent-mediated intragranular-coarsening of CH3NH3PbI3 thin films toward high-performance perovskite photovoltaics. ACS Appl Mater Interfaces 9:31959
7. Dubey A, Kantack N, Adhikari N, Reza KM, Venkatesan S, Kumar M, Khatiwada D, Darling S, Qiao Q (2016) Room temperature, air crystallized perovskite film for high performance solar cells. J Mater Chem A 4(26): 10231–10240
8. Adhikari N, Dubey A, Gaml EA, Vaagensmith B, Reza KM, Mabrouk SAA, Gu SP, Zai JT, Qian XF, Qiao QQ (2016) Crystallization of a perovskite film for higher performance solar cells by controlling water concentration in methyl ammonium iodide precursor solution. Nano 8(5):2693–2703
9. Khatiwada D, Venkatesan S, Adhikari N, Dubey A, Mitul A, Mohammad L, Iefanova A, Darling SB, Qiao QQ (2015) Efficient perovskite solar cells by temperature control in single and mixed halide precursor solutions and films. J Phys Chem C 119(46):25747–25753
10. Bi D, Moon S-J, Häggman L, Boschloo G, Yang L, Johansson Erik MJ, Nazeeruddin M-K, Grätzel M, Hagfeldt A (2013) Using a two-step deposition technique to prepare perovskite ($CH_3NH_3PbI_3$) for thin film solar cells based on ZrO_2 and TiO_2 mesostructure. RSC Adv 3:18762
11. Burschka J, Pellet N, Moon S-J, Robin H-B, Gao P, Nazeeruddin M-K, Grätzel M (2013) Sequential deposition as a route to high-performance perovskite-sensitized solar cells. Nature 499:316–319
12. Mo J, Zhang C, Chang J, Yang H, Xi H, Chen D, Lin Z, Lu G, Zhang J, Haoa Y (2017) Enhanced efficiency of planar perovskite solar cells via a two-step deposition using DMF as an additive to optimize the crystal growth behavior. J Mater Chem A 5:13032
13. Wang S, Yu W, Zhang L, Yang Y (2017) Crystallization process of PbI2 solution in two-step deposition of CH3NH3PbI3 for high-performance perovskite solar cells. Sol Energy Mater Sol Cells 161:444–448
14. Abzieher T, Mathies F, Hetterich M, Welle A, Gerthsen D, Lemmer U, Paetzold UW, Powalla M (2017) Additive-assisted crystallization dynamics in two-step fabrication of perovskite solar cells. Phys Status Solidi A 214: 1700509
15. Bahtiar A, Rahmanita S, Inayatie YD (2017) Pin-hole free perovskite film for solar cells application prepared by controlled two-step spin-coating method. IOP Conf Ser: Mater Sci Eng 196:012037
16. Huang J, Wang M, Ding L, Deng J, Yao X (2015) Efficiency enhancement of the $MAPbI_{3-x}Cl_x$-based perovskite solar cell by a two-step annealing procedure. Semicond Sci Technol 31(2):025009
17. Tress W, Marinova N, Moehl T, Zakeeruddin SM, Nazeeruddina MK, Grätzela M (2015) Understanding the rate-dependent J–V hysteresis, slow time component, and aging in $CH_3NH_3PbI_3$ perovskite solar cells: the role of a compensated electric field. Energy Environ Sci 8(3):995–1004

18. Wei J, Zhao Y, Li H, Li G, Pan J, Xu D, Zhao Q, Yu D (2014) Hysteresis analysis based on the ferroelectric effect in hybrid perovskite solar cells. J Phys Chem Lett 5(21):3937–3945
19. Bi E, Chen H, Xie F, Wu Y, Chen W, Su Y, Islam A, Grätzel M, Yang X, Han L (2017) Diffusion engineering of ions and charge carriers for stable efficient perovskite solar cells. Nat Commun 8:15330
20. Luo H, Lin X, Hou X, Pan L, Huang S, Chen X (2017) Efficient and air-stable planar perovskite solar cells formed on graphene-oxide-modified PEDOT: PSS hole transport layer. Nano-Micro Lett 9(4):39
21. Li B, Jiu T, Kuang C, Ma S, Chea Q, Li X, Fang J (2016) Chlorobenzene vapor assistant annealing method for fabricating high quality perovskite films. Org Electron 34:97–103
22. Tripathi N, Yanagida M, Shirai Y, Masuda T, Hanb L, Miyanoa K (2015) Hysteresis-free and highly stable perovskite solar cells produced via a chlorine-mediated interdiffusion method. J Mater Chem A 3(22): 12081–12088
23. Green M-A, Anita H-B, Snaith H-J (2014) The emergence of perovskite solar cells. Nat Photonics 8:506–514